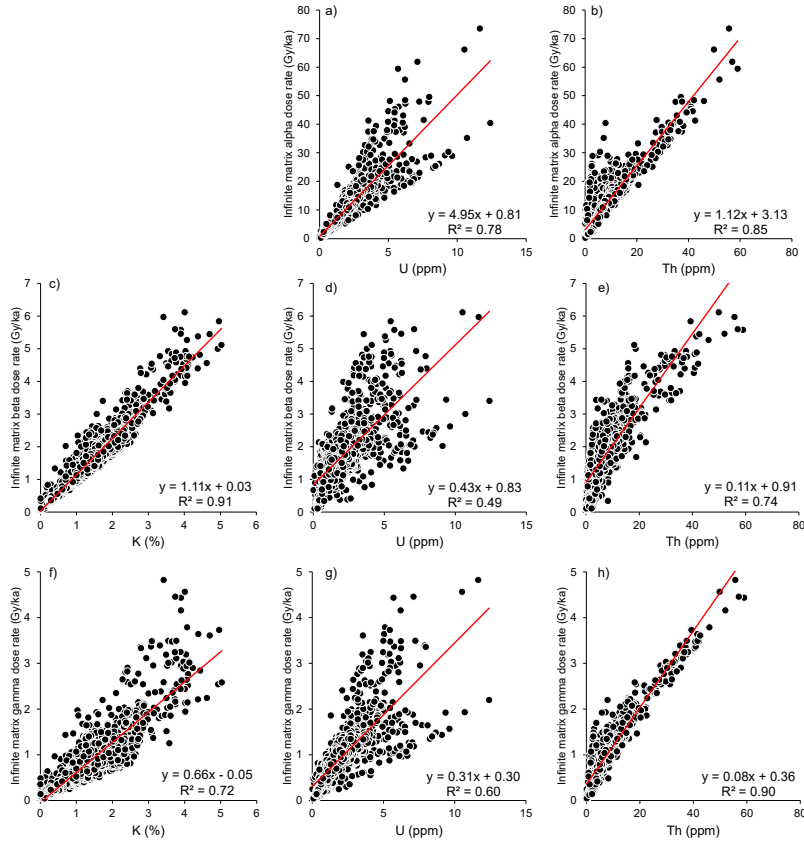


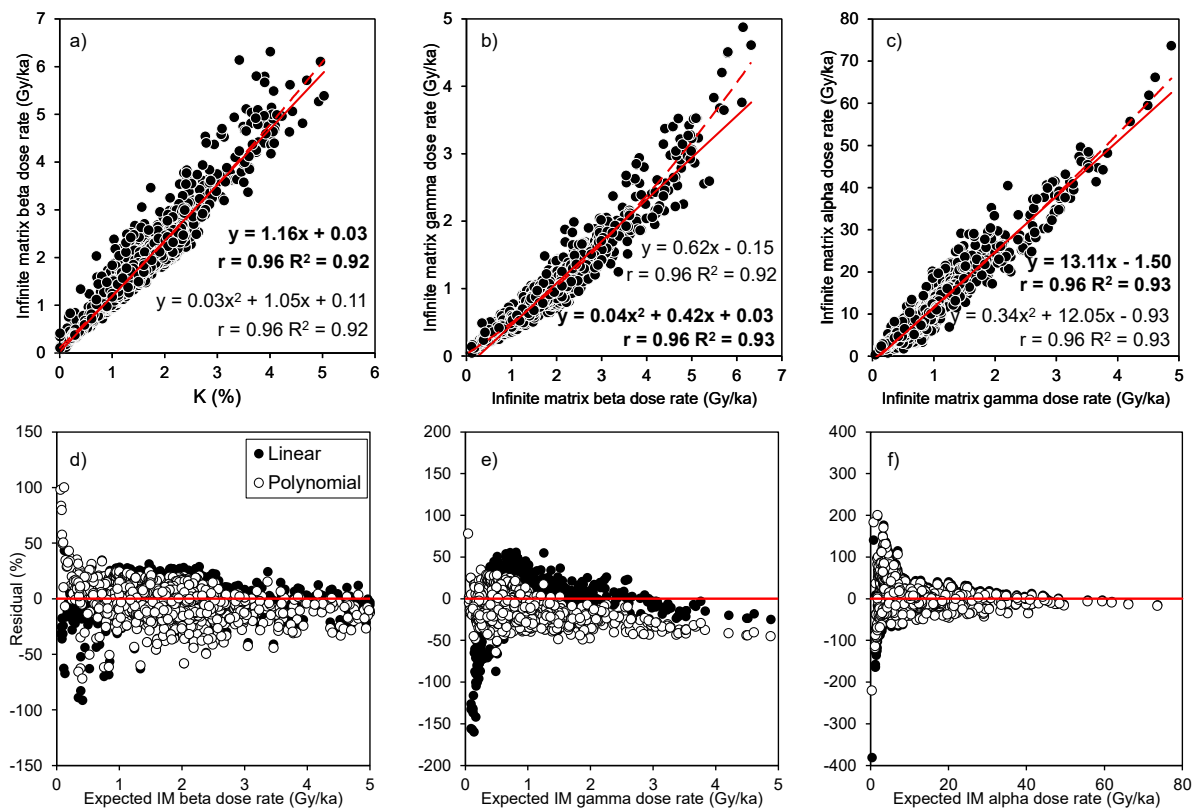
## S1. Radionuclide dataset

Figure S1 shows the linear relationships between individual radionuclides (K, U and Th) and external infinite matrix dose rates from the radionuclide dataset compiled in this study. The IM  $\dot{D}_\alpha$  scales most strongly with Th concentration ( $R^2 = 0.85$ ). The IM  $\dot{D}_\beta$  scales most strongly with K concentration ( $R^2 = 0.91$ ). The IM  $\dot{D}_\gamma$  scales most strongly with Th concentration ( $R^2 = 0.90$ ).

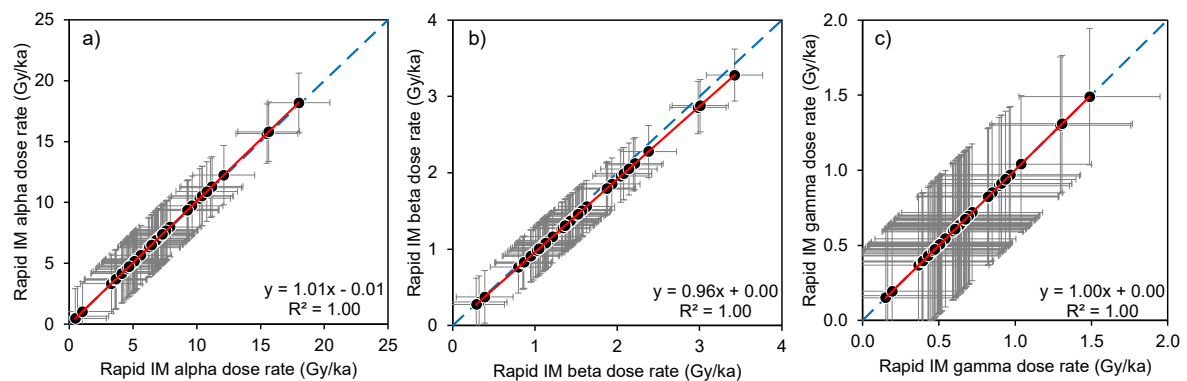


**Figure S1.** Linear relationships between radionuclides and infinite matrix dose rates for a-b) IM alpha dose rate ( $\dot{D}_\alpha$ ), c-e) IM beta dose rate ( $\dot{D}_\beta$ ), and f-h) IM gamma dose rate ( $\dot{D}_\gamma$ ). Data were compiled from the training dataset ( $n = 1473$  in all plots), with IM dose rates calculated using the radionuclide conversion factors of Guerin et al. (2011).

Figure S2 (a-c) shows the results of IM  $\dot{D}_\alpha$ ,  $\dot{D}_\beta$  and  $\dot{D}_\gamma$  calculated from the K, U and Th values comprising the 1473 sample radionuclide dataset and the conversion factors of Cresswell et al. (2018). The resulting linear and polynomial regression equations are very similar to those shown in Figure 4 of the main text, calculated using the conversion factors of Guerin et al. (2011). Consequently, the rapid infinite-matrix dose rates predicted based on the pXRF K concentrations measured for the samples in the main text using these alternative regression relationships are identical to those calculated based on the regression relationships in the main text (Fig. S3). Therefore, users can choose whichever of these two conversion factors they prefer for rapidly



19  
20 **Figure S2.** Regression relationships for: a) K concentration and IM  $\dot{D}_\beta$ , b) IM  $\dot{D}_\beta$  and IM  $\dot{D}_\gamma$ , and c) IM  $\dot{D}_\gamma$  and IM  $\dot{D}_\alpha$   
21 calculated using the conversion factors of Cresswell et al. (2018). Equations in bold denote the most appropriate  
22 model fits, based on the residuals. Solid red lines denote the linear trendlines and dashed red lines denote the second  
23 order polynomial trendlines ( $n=1473$ ). Pearson's correlation coefficient ( $r$ ) and  $R^2$  values are given for each relationship.  
24 The root mean squared errors (RMSEs) of the linear relationships are a) 0.29, b) 0.18, and c) 2.38 Gy/ka. The RMSEs of  
25 the polynomial relationships are a) 0.31, b) 0.31 and c) 2.43 Gy/ka. Panels d-f show the residuals of the relationships  
26 in a-c, expressed as a percentage of the expected dose rate, in each case plotted against the expected dose rate  
27 calculated with high-precision methods.



28  
29 **Figure S3.** Results of the IM external dose rates calculated using the regression relationships given in Fig.S2 (based on  
30 the conversion factors of Cresswell et al., 2018; x-axes) and the regression relationships given in Figure 4 of the main  
31 text (based on the conversion factors of Guerin et al., 2011; y-axes): a) IM  $\dot{D}_\alpha$  results, b) IM  $\dot{D}_\beta$  results, c) IM  $\dot{D}_\gamma$  results.

## 32 S2. Portable XRF measurements

33 Table S1 shows the five certified reference materials (CRMs) with independently measured K  
34 concentrations that were used to calibrate the pXRF measurements. These CRMs were chosen  
35 as they have K concentrations that reflected the range of interest as closely as possible, based

on the K concentrations of the samples included in this study (see separate .csv file in the supplementary data). Reference material OREAS76b has the lowest K concentration, so was used to calculate the limit of detection (LOD) and limit of quantification (LOQ) for K on our instrument (Le Vaillant et al., 2014; Andrew and Barker, 2018). The LOD is reported as three times the standard deviation of fifteen repeat measurements of OREAS76b, whereas the LOQ is equal to ten times the standard deviation of these fifteen repeat measurements (Le Vaillant et al., 2014).

A linear equation was used to calibrate pXRF measurements by taking the mean K concentration of fifteen repeat measurements of each CRM and plotting them against their independently verified K concentration (Table S1; Andrew and Barker, 2018). The calibration equation is shown in Figure S4.

**Table S1.** The chosen CRMs and the means and standard deviations of the fifteen repeat measurements used to derive the calibration equation (Fig.S2). The LOD and LOQ are calculated for OREAS76b as it has the lowest K concentration of the CRMs.

| CRM      | Matrix                   | High-precision K (%) | Measurement method | pXRF K (%) | 1 $\sigma$ (%) | LOD   | LOQ   |
|----------|--------------------------|----------------------|--------------------|------------|----------------|-------|-------|
| OREAS76b | Ultramafic               | 0.47                 | Fusion XRF         | 0.40       | 0.005          | 0.015 | 0.049 |
| OREAS30a | Basalt                   | 1.68                 | Fusion ICP         | 1.24       | 0.019          | -     | -     |
| OREAS752 | Pegmatite                | 2.10                 | Fusion ICP         | 2.01       | 0.007          | -     | -     |
| OREAS20a | Granodiorite             | 3.34                 | Fusion ICP         | 2.87       | 0.013          | -     | -     |
| OREAS130 | Sulfidic graphitic slate | 4.96                 | Fusion ICP         | 4.64       | 0.013          | -     | -     |

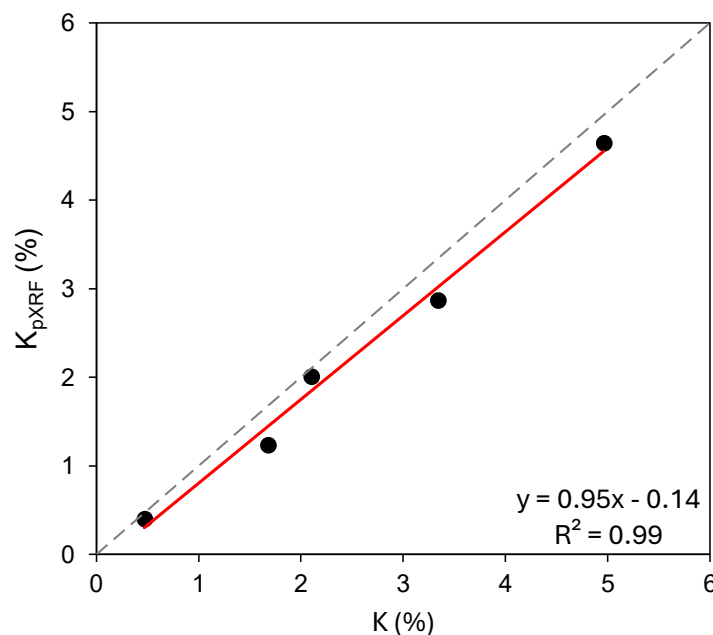


**Figure S4.** The relationship between the mean K concentrations of the CRMs measured using the pXRF (y axis) and their known K concentrations (x axis). The linear equation of this relationship was used to calibrate measurements of K concentration in this study. The standard errors of the gradient and intercept of this relationship are 0.06 and 0.17, respectively. The dashed line represents unity.

### S3. Simplified attenuation procedure

Figure S5 shows that very little noise is contributed to rapidly predicted total dose rates because of using the simplified attenuation procedure for attenuating infinite-matrix dose rates (Table 3). In all cases,  $R^2 = >0.99$ .

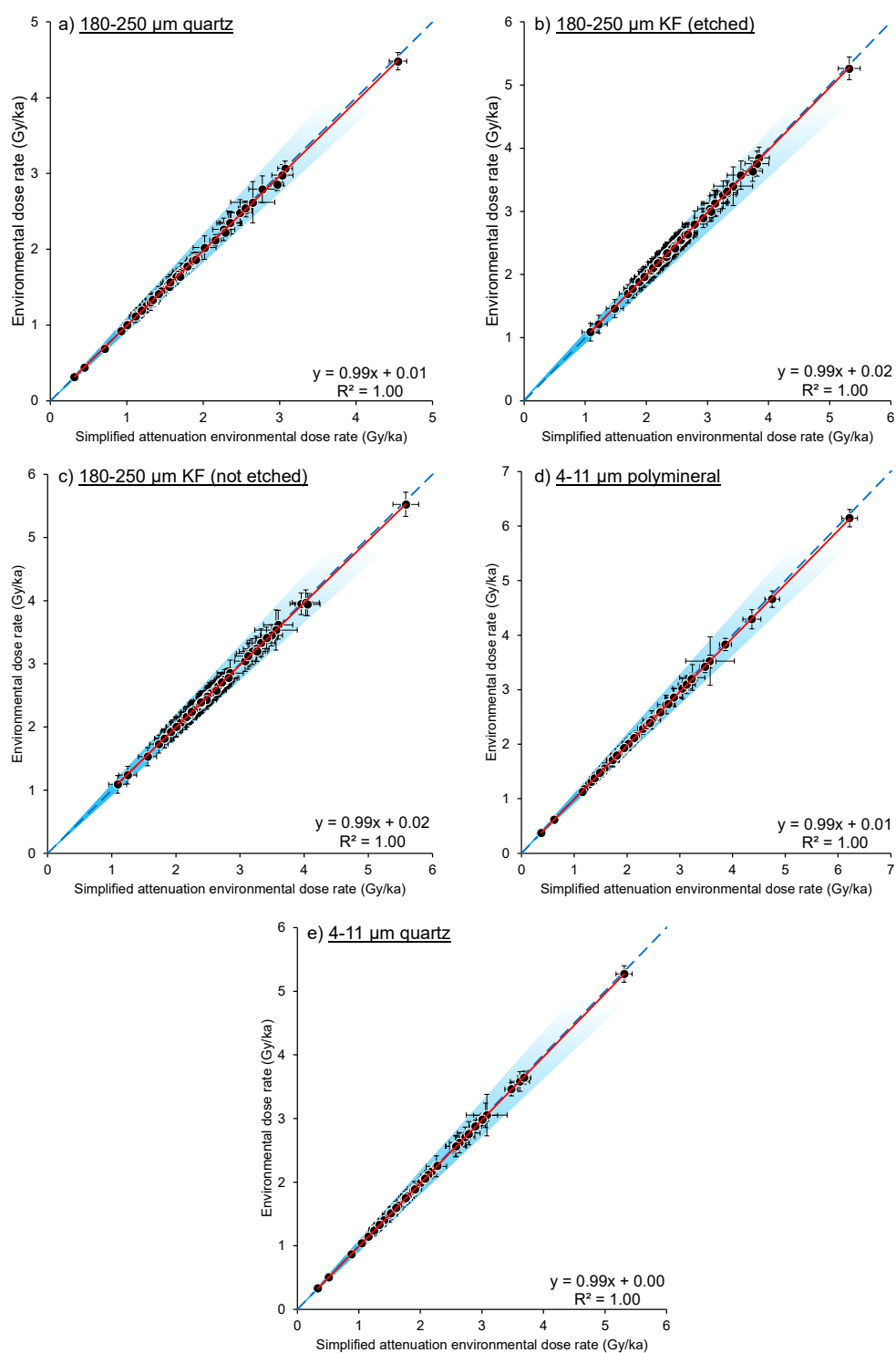


**Figure S5.** Total dose rate calculated with the simplified attenuation procedure (x-axes) and total dose rates calculated using full correction in the DRAC software (y-axes) for: a) 180-250  $\mu\text{m}$  quartz, b) 180-250  $\mu\text{m}$  K-feldspar (etched), c) 180-250  $\mu\text{m}$  K-feldspar (not-etched), d) 4-11  $\mu\text{m}$  polyminerals and e) 4-11  $\mu\text{m}$  quartz. In both cases, IM dose rates were

calculated from high-precision K, U and Th data. The dashed blue lines and blue shaded areas represent unity  $\pm 10\%$ , respectively. The red lines denote the linear trendline for each dataset ( $n = 66$  in all cases). The standard errors of the regression slopes and intercepts are a)  $\pm 0.05$  and  $\pm 0.08$ , b)  $\pm 0.05$  and  $\pm 0.12$ , c)  $\pm 0.05$  and  $\pm 0.13$ , d)  $\pm 0.06$  and  $\pm 0.16$  and e)  $\pm 0.05$  and  $\pm 0.11$ .